# The effect of He-ash-poisoning on the L-mode and the high β_p-mode confinements and its application to ITER-like plasma

Tateishi, Gonta
Interdisciplinary Graduate School of Engineering Sciences, Kyushu University

Itoh, Sanae-I.
Research Institute for Applied Mechanics, Kyushu University

Yagi, Masatoshi
Research Institute for Applied Mechanics, Kyushu University

https://doi.org/10.5109/6786350

出版情報：Reports of Research Institute for Applied Mechanics. 43 (115), pp.57-85, 1997-09. 九州大学応用力学研究所

Reports of Research Institute for Applied Mechanics
Vol. XLIII No. 115, 1997

# The effect of He-ash-poisoning on the L-mode and the high $\beta_p$-mode confinements and its application to ITER-like plasma

By Gonta TATEISHI†, Sanae-I. ITOH* and Masatoshi YAGI*

The burning performance of the self-ignited steady plasma is investigated by use of point model. For the ITER-like parameters, the theoretical model scaling law, that can explain the L-mode and the high $\beta_p$-mode, is employed. The effect of He-ash-poisoning is introduced simultaneously. The solutions of particle and energy balances for the steady state are obtained in the presence of the effect of radiation loss due to He-ash and fuel ions. There found at most four solutions for the plasma current at fixed temperature. The L-mode branches (two solutions of high current regime) and the high $\beta_p$-mode (two solutions of low current regime) branches are well separated on the plane of the current and the temperature in the low density regime. The merging of two branches occurs in the higher density regime due to the nonlinear effect contained in the scaling law. It is shown that the divergence of the temperature, which has been expected for the pure plasma in the high $\beta_p$-mode, disappears under the influence of He-ash. Examining the constraints imposed to the plasma (the density limit, the $\beta_p$ limit, and so on), we found that the core self-ignited state of the high $\beta_p$-mode operation would be difficult.

***Key words***: self-ignition, He-ash, High $\beta_p$—mode, ITER, plasma

## Contents



† Interdisciplinary Graduate School of Engineering Sciences, Kyushu Univ.
* Research Institute for Applied Mechanics, Kyushu Univ.

## I. Introduction

In a self-ignited plasma, the existence of the thermal instability has been expected and it has been reported that the unstable condition for the thermal instability is determined by the balance between the fusion input and the power loss which is characterized by the energy confinement time $\tau_E$ [1]. As for an effective control of this thermal instability, the suppression of increment of the temperature by the plasma movement in the direction of major radius [2], or the positive control of compression and expansion of the plasma by the vertical magnetic field [3, 4] have been investigated. Taking advantage of the ripple loss of fast $\alpha$-particles, the stabilization by the control of $\alpha$-deposition profile has also been proposed [5]. The stabilization by the pellet injection has also been investigated [6]. On one hand the self-ignition condition has been reported to be affected by the effect of fuel dilution [7] and the scaling law of the energy confinement time $\tau_E$. The generation of $\alpha$-particles, the production of He-ash through the slowing down process, and its impact on pumping requirements, the burn condition and the minimum reactor size have also been considered in several publications (e. g. Ref. [8-14]). Comparisons between TRANSP simulations [15] and diagnostic measurements of confined and escaping $\alpha$-particles [16, 17] and of He-ash have suggested that the $\alpha$-particle behavior could be neoclassical in the absence of large scale MHD if orbit effects including ripple losses [18] are taken into account. It is reported that in the large size tokamak such as ITER with the large current ($I_p \sim 21$MA [19]), most of $\alpha$-particles can be confined, in the sense of single particle orbit, as long as the axisymmetry can be assumed [20].

In all tokamaks, it is observed that the energy confinement time $\tau_E$ is degraded as the heating power $P_{in}$ increases, what is called 'L-mode' confinement. Efforts have been made on the regression analysis of the global confinement time $\tau_E$ [21, 22]. Various kinds of enhanced confinement mode have also been observed in tokamaks, and the self-ignition condition is expected to be achieved using operations with these modes in future experimental tokamaks such as in ITER [19], [23]. When a bootstrap fraction is large enough, the high $\beta_p$-mode is triggered and the energy confinement time is enhanced about 2 or 3 times larger than that of L-mode [24]-[30]. Here a bootstrap fraction indicates the ratio of the bootstrap current to the total current.

A new theory has been proposed to determine the transport coefficient based on nonlinear MHD instability [31, 32]. This theory explains, at least qualitatively, various aspects of the L-mode and the high $\beta_p$-mode plasmas, including the influence of the current profile and magnetic shear [33]. In this new approach, the turbulence is sustained by the anomalous transport induced by the turbulence itself, i.e., the nonlinear destabilizing and stabilizing effects of the anomalous transport on the fluctuations are included.

The scaling law for the energy confinement time which covers both the L-mode and the high $\beta_p$-mode has been obtained by numerical simulations based on this model [34]. In the condition for the self-ignited state, it has been reported that if this scaling is employed, there can be a divergence of the temperature due to the nonlinear interaction between the plasma current $I_p$ and the temperature $T$ on the high $\beta_p$-mode [35]. However in this model scaling, the fuel dilution by He-ash and the energy losses by radiations have not been considered consistently. In order to examine the core performance of ignited plasma, it is inevitable for the analysis of thermal stability to take these effects into account.

The operational window where the steady burning plasma satisfies various kinds of the constraints (i. e., the limits for the plasma $\beta$ value which represents plasma diamagnetism and is defined as the ratio of the plasma pressure to the magnetic pressure, for the safety factor, and for the density, the current drive-efficiency, the low temperature divertor and the ash pumping) has been investigated using the empirical L-mode scaling law [36]. The burning performance should also be examined from this aspect.

The organization of this paper is as follows. In Sec. II, we review the thermal instability and its stabilization. The typical works about the ash-contamination and the energy confinement times are shown. Previous analysis of the operational window for the self-ignited plasma is briefly discussed. In Sec. III, we include the effects of dilution due to He-ash and the energy loss due to radiation, and examine the thermal stability of the L-mode and the high $\beta_p$-mode comfinements. First, basic equations and assumptions are shown. Next we show that the effect of ash-poisoning on the self-ignition condition qualitatively. The analysis is also applied to the ITER-grade tokamak. We discuss the core plasma characteristics taking the presently argued operational limits, (e.g., the density limit) into account and compare burning performances of the L-mode with the high $\beta_p$-mode. Summary and discussion are given in Sec. IV.

## II. Reviews

### II-1. The thermal instability and its stabilization

In this section we survey the thermal instability and its stabilization. The plasma is assumed to contain deuterium and tritium as one to one mixture and no impurities. It is also assumed that the $\alpha$-particles give their whole initial energy to the plasma as soon as they are produced by D-T fusion reaction. Setting the plasma temperature as $T_i = T_e = T$, the energy balance equation based on the point model is given as follows

$$\frac{dW_p}{dt} = -\frac{W_p}{\tau_E} + Q_\alpha - Q_{br}, \tag{2.1}$$

where $W_p$ is the plasma energy density defined by $3n_eT$ with the plasma density $n_e$, $\tau_E$ is the energy confinement time. The value $Q_\alpha$ is the $\alpha$-heating power defined by $\frac{1}{4}n_e^2\langle\sigma v\rangle E_\alpha$ where $\langle\sigma v\rangle$ represents the D-T reaction rate and $E_\alpha$ is the initial energy of $\alpha$-particle with $E_\alpha=3.5$ MeV. The value $Q_{br}$ is the radiation power loss (bremsstrahlung). A definite formula of $Q_{br}$ will be explained in Sec. III. Setting the R.H.S of Eq. (2.1) to be zero, we obtain the self-ignition condition for the steady state as

$$-\frac{W_{p0}}{\tau_{E0}}+Q_{\alpha 0}-Q_{br0}=0, \tag{2.2}$$

Where the subscription 0 indicates the equilibrium variable. Assuming $n_e=$ const. and linearizing Eq. (2.1) around the value of equilibrium determined by Eq. (2.2), we obtain the growth rate of thermal instability,

$$\gamma_T=\frac{E_\alpha}{12}n_{e0}\frac{d\langle\sigma v\rangle}{dT}-\frac{1}{\tau_{E0}}\left(1-T_0\frac{\partial}{\partial T}\ln(\tau_{E0})\right)-\frac{1}{3n_{e0}}\frac{\partial Q_{br}}{\partial T}. \tag{2.3}$$

Condition $\gamma_T>0$ means, the equilibrium point is unstable for the perturbation. The reaction rate $\langle\sigma v\rangle$ has the nonlinear dependence of the temperature which is given by [37]

$$\langle\sigma v\rangle=3.7\times10^{-18}\cdot\frac{1}{h\cdot T^{2/3}}\exp\left(-\frac{20}{T^{1/3}}\right) \qquad [m^3/s], \tag{2.4}$$

where

$$h=\frac{T}{37}+\frac{5.45}{3+T\{1+(T/37.5)^{2.8}\}}.$$

The thermal instability is driven by the temperature dependence of the reaction rate, i.e., the first term of Eq. (2.3). The unstable condition is determined by the balance between the temperature dependences of $\langle\sigma v\rangle$, $\tau_E$, and $Q_{br}$.

The stability analysis with a specific scaling law of $\tau_E$ has been investigated [1] without the radiation power loss. Taking advantage of the ripple loss of fast $\alpha$-particles, stabilization by the control of $\alpha$-deposition profile has been also proposed [5]. If the plasma temperature increases, the plasma shifts outwardly and the effect of toroidal ripple is strengthened. Consequently the confinement of $\alpha$-particles is degraded and the plasma recovers the equilibrium by the decrease of $\alpha$-heating. The strong $\beta_p$ dependence of ripple energy loss has been reported that the loss fraction is proportional to $\beta_p^{5.7}$, where the $\beta_p$ value is defined by

$$\beta_p=\frac{\int p dV}{VB_p(a)^2/2\mu_0}$$

where $\int dV$ means the volume integral, $p$ is the pressure, $V$ is the total plasma volume ($=2\pi^2a^2R$, for the circular cross section), and $B_p(a)$ is the strength of poloidal magnetic field at $\gamma=a$. The thermal stability is affected by the competition between $\alpha$-heating, Shafranov shift and ripple loss.

The stabilization by the pellet injection has also been investigated [6]. The pellets are used to control the thermal instability. One-dimensional transport simulation was done in which the abrupt decrease of plasma power is caused by injected He-pellet(impurity). The melting of pellets by the high energy ions is considered in this pellet model, and the fusion power output decreases half of it.

## II-2. The confinement of $\alpha$-particles and He-ash-contamination in tokamak

Preliminary experimental data indicates that the slowing down process and transport of fast ions, such as $\alpha$-particles, are not inconsistent with the neoclassical collisional theory, though this needs careful checking by comparison of calculated distribution functions with measured ones.

Figure 1 shows the plasma current versus the aspect ratio on the condition that whole of $\alpha$-particle can be confined absolutely in the radius normalized by the minor radius of tokamak, assuming that the magnetic field is axisymmetric, the plasma current density is uniform, and the $\alpha$-particle production rate

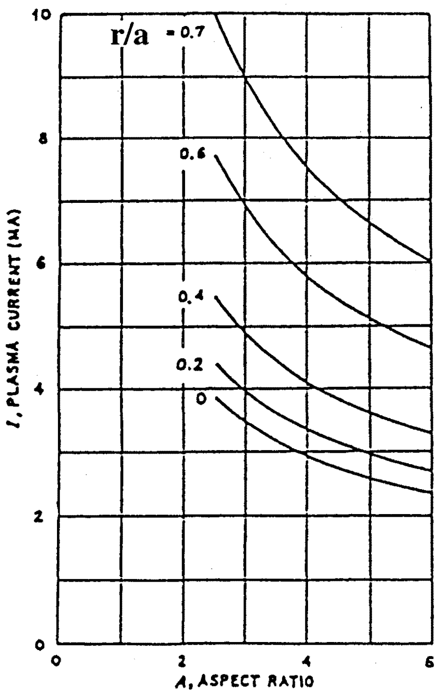


Fig. 1 Required plasma current for absolute trapping of $\alpha$-particle (cited from Ref. [20] )

depends only on the radial location r (cited from [20]). It is found that in the large current tokamak such as ITER ($I_p \sim 21$MA [19]), the confinement for the absolute trapping of $\alpha$-particles is fairly good, therefore the sufficient $\alpha$-heating could be expected as long as the axisymmetric magnetic field is assumed.

The bootstrap current and the electric conductance which are determined by the force balance in the direction of the magnetic field also seem to be comparable to the prediction of neoclassical theory [38]. However, the particle flux and the heat diffusion which are observed in tokamak are actually much larger than that predicted by neoclassical theory.

We assume that $\alpha$-particles are conrfined perfectly and give their whole energy to the bulk plasma, and that they become the He-ash. Let us explain the accumulation of He-ash. The global He-ash confinement time $\tau_\alpha^*$ is defined as

$$\tau_\alpha^* = \frac{N_\alpha}{\Phi_{\alpha,out} - \Phi_{\alpha,ret}} \tag{2.5}$$

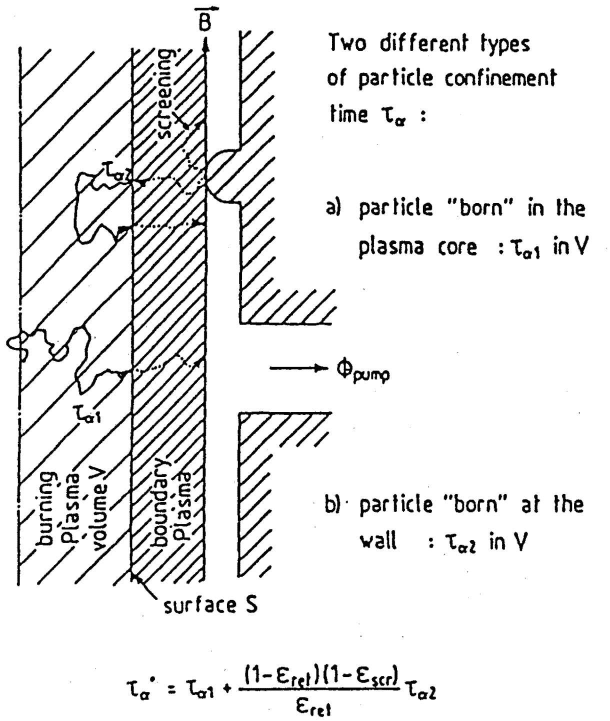


Fig. 2 Helium exhaust : model and definitions for a pumped limiter (similar definitions apply to a divertor, cited from Ref. [7] ).

where $N_\alpha$ is the number of He-ash in the burning region with volume $V$, and the exhaust flux $\Phi_{\alpha,out}-\Phi_{\alpha,ret}$ is the net flux of He-ash leaving this region through the surface $S$ (Fig. 2) (cited from [7]), which is defined by the difference between outward and returning flux, $\Phi_{\alpha,out}$ and $\Phi_{\alpha,ret}$, respectively. Obviously, $\tau_\alpha^*$ can become significantly larger than the usual He-ash confinement time, $\tau_\alpha = N_\alpha/\Phi_{\alpha,out}$. We can define two kinds of He-ash according to the location of their sources. One species consists of the first generation He-ash, i.e. of particles born in the plasma core by fusion events before they leave the burning region for the first time. The second species comprise of particles which have been recycled to the burning region by processes described by an effective recycling coefficient $R_{eff}$. Considering these, the global He-ash confinement time $\tau_\alpha^*$ can be rewritten as [7]

$$\tau_\alpha^* = \tau_{\alpha 1} + \frac{R_{eff}}{1-R_{eff}}\tau_{\alpha 2}, \tag{2.6}$$

where $\tau_{\alpha 1}$ is the internal He-ash confinement time, $\tau_{\alpha 2}$ is the mean residence time.

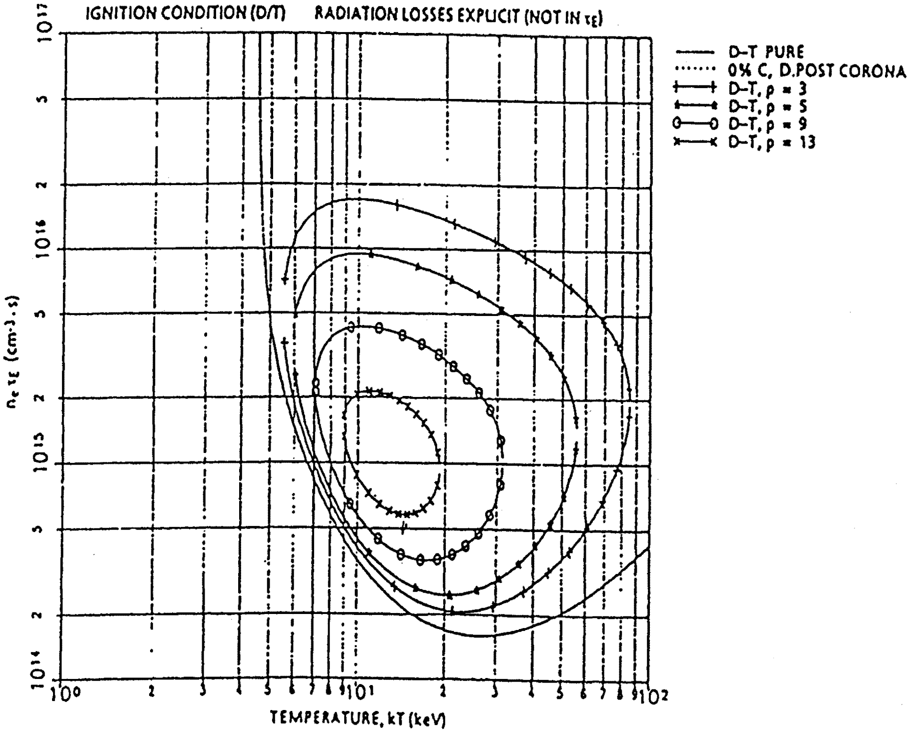


Fig. 3 Ignition parameters $n_e\tau_E$ in burning D-T plasma as functions of $T$ and $\rho$ with no impurities except He (cited from Ref. [7] ).

The effective He-ash exhaust efficiency $\varepsilon_{eff}$ is defined by $\varepsilon_{eff}=1-R_{eff}$, and $\varepsilon_{eff}$ $\sim$0.1 seems to be achievable with divertor and other configurations. Introducing the constant parameter $\rho$ as $\rho=\tau_{\alpha}^{*}/\tau_{E}$, which represents the effect of the fuel dilution, the self-ignition condition for D-T plasma is analytically derived from the energy balance and the He-ash particle balance [7].

Figure 3 shows the ignition condition for various values of $\rho$ (cited from [7]). For an ignited and stationary burning D-T plasma, this ratio needs to remain sufficiently below 15 for typical impurity concentrations.

### II-3. Scaling laws for the energy confinement time and the thermal instability

Empirical scaling laws for the energy confinement time have been derived using experimental databases. Many scaling laws have been proposed, such as Goldston's scaling law for the L-mode plasmas [21]. The ITER group has investigated them further [22]. The scaling law for the L-mode confinement is given by

$$\tau_E^{ITER89-P}=0.048M^{0.5}I_p^{0.85}R^{1.2}a^{0.3}K_{95}^{0.5}\bar{n}^{0.1}B_t^{0.2}P_{in}^{-0.5}, \tag{2.7}$$

where $M$ is the average isotopic mass number, $I_p$ is the plasma current in [MA], $R$ is the major radius in [m], $a$ is the minor radius in [m], $\varkappa_{95}$ is the elongation at the plasma surface, $\bar{n}$ is the line averaged plasma density in units of $[10^{20}m^{-3}]$, $B_t$ is the toroidal field in [T] and $P_{in}$ is the total plasma heating power in [MW].

A new theoretical formula has been proposed based on the self-sustained plasma turbulence due to the current diffusive ballooning mode, and has succeeded to explain the characteristics of the L-mode.

By solving the eigenvalue problem for the current diffusive ballooning/interchange mode, a general expression of the turbulent thermal diffusivity $\chi_{TB}$ [31, 32] is estimated by

$$\chi_{TB}=F(s,\alpha,\varkappa)|\alpha|^{3/2}\frac{c^2\nu_A}{\omega_{pe}^2qR}, \tag{2.8}$$

where $c$ is the velocity of light, $\omega_{pe}$ is the electron plasma frequency, $\nu_A$ is the toroidal Alfven velocity, $q$ is the safety factor. The geometrical factor $F$ is a function of the magnetic shear $s$, the normalized pressure gradient $\alpha$, and the magnetic curvature $\varkappa$, they are defined by

$$s\equiv\frac{rdq}{qdr}, \tag{2.9}$$

$$\alpha\equiv-q^2R\frac{d\beta}{dr}, \tag{2.10}$$

and

$$\varkappa\equiv-\frac{a}{R}\left(1-\frac{1}{q^2}\right), \tag{2.11}$$

where $\beta$ is the ratio of the total plasma pressure to the magnetic pressure, $2\mu_0(p_e + p_i)/B_t^2$. The strong $\nabla T$ dependence on the heat flux, $q \propto (\nabla T)^{5/2}$ is consistent with the nonlinear $\nabla T$ dependence of the heat flux observed on the JET tokamak [39]. The $\nabla n_e$ dependence explains the finite thermal diffusivity around $\nabla T=0$. A similar expression of the thermal diffusivity, proportional to $\alpha$, has been proposed by Taroni in order to explain the local and global energy confinement of the L-mode plasmas in JET [40].

For the current diffusive ballooning mode turbulence in a tokamak with a circular cross section, an analytical expression for the geometrical factor $F$ is obtained [41] by

$$F(s, \alpha, \varkappa)=\frac{(1+\varkappa)^{5/2}}{\sqrt{2(1-2s')[1-2s'+3s'^2(1+\varkappa)]}}, \text{ for } s' << 1/2 \tag{2.12}$$

where $s' \equiv s-\alpha$.

The numerical solution of the eigenvalue equation gives the contour plot of $\chi$ as shown in Figure 4 (cited from [35]). This figure shows the case of $\varkappa=-0.1$ and $c^2/\omega_{pe}^2 a^2=10^{-4}$, where $\chi$ denotes the normalized $\chi$ using $(c/a^2)(qR/\nu_A)$. The broken curve indicates the stability boundary of the high-n ballooning mode predicted by the ideal MHD theory with $\hat{\chi}=0$. For the strong shear case ($s \sim 1$), $\hat{\chi}$ increases rapidly with the increase of $\alpha$. On the other hand, the increase of $\alpha$ is gradual for the case of weak shear or the negative shear ($s \leqq 1/2$). This is because the driving force of the current diffusive ballooning mode is reduced

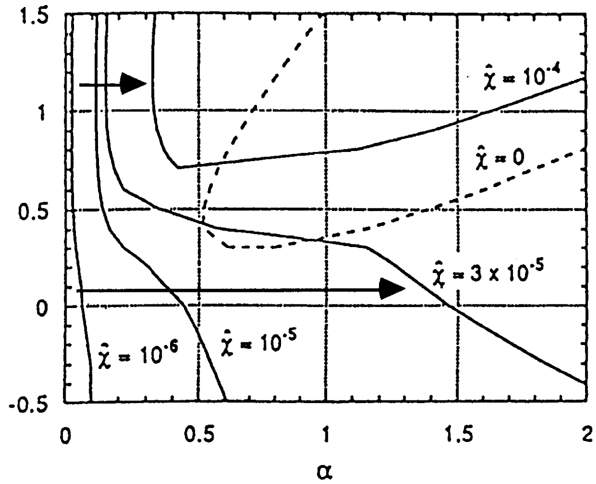


Fig. 4 Contour of the turbulent transport coefficient in the $s-\alpha$ plane: $\hat{X}$ denotes the thermal transport coefficient normalized to $a^2\nu_A/qR$. (Other paramaters: $R/r=8$, $q=3$, and $a^2\omega_p^2/c=10^4$). (cited from Ref. [35]).

owing to the increase of $\alpha$ in the second stability region [42].

Assuming to be $|\varkappa|<<1$, the following interpolated formula of the geometrical factor for the current diffusive ballooning mode has been obtained by using numerical results,

$$F_{BM}=\frac{1}{\sqrt{2(1-2_{s}')[1-2s'+3s'^{2}]}} \qquad (s'<0), \tag{2.13}$$

$$=\frac{(1+9\sqrt{2}s'^{5/2})}{\sqrt{2}(1-2s'+3s'^{2}+2s'^{3})} \qquad (s'>0).$$

In the case of magnetic hill configuration ($q<1$), the current diffusive interchange mode turbulence is possible. The analytical expression of the factor $F$ for this mode has been given by [31]

$$F_{IM}=\frac{1}{s^{2}}\left(\frac{R}{a}\varkappa\right)^{3/2} \qquad (\varkappa>0), \tag{2.14}$$

$$=0 \qquad (\varkappa<0).$$

Since the mode with higher saturation level dominates the anomalous transport, it is assumed that the greater one of the two factors effective, i. e.,

$$F(s,\ \alpha,\ \varkappa)=\max(F_{BM},\ F_{IM}). \tag{2.15}$$

In the numerical simulation, the transport code TASK/TR [43] was employed with several assumptions to simplify the analysis and elucidate the mechanism of the thermal transport.

The one-dimensional transport equations are given by

$$\frac{\partial}{\partial t}\left(\frac{3}{2}n_{e}T_{e}\right)=-\frac{1\partial}{r\partial r}rn_{e}\chi_{e}\frac{\partial T_{e}}{\partial r}+P_{OH}+P_{ie}+P_{He}, \tag{2.16}$$

$$\frac{\partial}{\partial t}\left(\frac{3}{2}n_{i}T_{i}\right)=-\frac{1\partial}{r\partial r}rn_{i}\chi_{i}\frac{\partial T_{i}}{\partial r}-P_{ie}+P_{Hi}, \tag{2.17}$$

and

$$\frac{\partial}{\partial t}B_{\theta}=\frac{\partial}{\partial r}\eta_{NC}\left[\frac{1}{\mu_{0}}\frac{1}{r}\frac{\partial}{\partial r}rB_{\theta}-J_{BS}-J_{LH}\right]. \tag{2.18}$$

where $P_{OH}$ denotes the Joule heating power, $P_{ie}$ the equipartition power, $P_{He}$ and $P_{Hi}$ the additional heating power, respectively. The magnetic diffusion equation includes the neoclassical resistivity $\eta_{NC}$, the bootstrap current $J_{BS}$ and the current $J_{LH}$ driven by the lower-hybrid-wave.

The density profile is fixed in time in the following form:

$$n_{e}(r)=n_{e0}\left(1-\frac{r^{2}}{a^{2}}\right)^{1/2} \tag{2.19}$$

The heating profile is assumed to be Gaussian,

$$P_{in}(r)=P_{in0}\exp\left[-\frac{(r-r_{HO})^{2}}{r^{2}_{HW}}\right], \tag{2.20}$$

with $r_{HO}=0$ and $r_{HW}=a/2$ for standard calculation, Effects of impurities, neutral particles and sawtooth oscillations are neglected.

The thermal transport coefficients are given as a sum of the turbulent term $\chi_{TB}$ and the neoclassical term $\chi_{NC}$. Since the electron and ion thermal diffusivities are not separated in the present turbulence model, it was assumed that they have the same magnitude, The thermal diffusivities are given by

$$\chi_e = \chi_{NCe} + C\chi_{TB}, \tag{2.21}$$

$$\chi_i = \chi_{NCi} + C\chi_{TB}. \tag{2.22}$$

where $C$ is the adjusting parameter. The neoclassical formula of $\chi_{NC}$, $J_{BS}$ and $\eta_{NC}$ are employed according to Ref. [44]. $C$ is determined to be $C \sim 12$ by comparing the calculated energy confinement time for the standard plasma parameters ($R=3$m, $a=1.2$m, $\varkappa=1.5$, $B_t=3$T, $I_p=3$MA, central electron density $n_e(0)=5\times10^{19}m^{-3}$, heating power $P=10$MW with $P_{He}=P_{Hi}$, for deuterium plasma) with the ITER-89P L-mode scaling law [22].

The global energy confinement time $\tau_E$ for current diffusive ballooning turbulence can be estimated from zero-dimensional energy balance as

$$\tau_E \propto a^{0.4} R^{1.2} I_p^{0.8} P_{in}^{-0.6} M^{0.2} F^{-0.4} n_e^{0.6} l_p^{0.6}, \tag{2.23}$$

where $l_p$ is the pressure scale length. This result agrees well with the L-mode scaling [21, 22] except the $n_e$ and a dependence.

This model is extended to the improved confinement mode called high $\beta_p$-mode, which appears when the large amount of bootstrap current is induced. In this case, the interpolated formula for $\tau_E$ is obtained by $\tau_E = f_\tau L^{2.2} I_p^{0.8} n_e^{0.6} P_{in}^{-0.6}\left(1 + \beta_p^4\right)^{0.2}$, where $L$ is the characteristic size of the system, $f_\tau$ indicates a numerical coeffcient. The $\beta_p$ dependence in the brackets represents the confinement improvement by the change of the current profile associated with bootstrap current generation. In the limit of $\beta_p \to 0$, this model reduced to the L-mode formula Eq. (2.7).

Figure 5 shows the improvement factor of the energy confinement time as a function of $\beta_p$ for various currents and heating power (cited from [34]). The improved confinement is reproduced by this model seen in Fig. 5. Considering the definition of the energy confinement time, i. e., $\tau_E = \frac{n_e T L^3}{P_{in}}$, the dependence of $\tau_E$ on the heating power can be rewritten as a dependence on the plasma temperature:

$$\tau_E = f_\tau^{2.5} L I_p^2 T^{-1.5} (1+\beta_p^4)^{0.5} \tag{2.24}$$

where the plasma volume is replaced by $L^3$. Based on this transport model, a new type of thermal instability has been investigated, which is driven by the nonlinear link between the transport coefficient, plasma profiles and the $\alpha$-heating power. Hereafter we follow the procedure described in Ref. [35]. For simplicity, the relation, $n_D = n_T = n_e/2$ is assumed. The temperature dependence

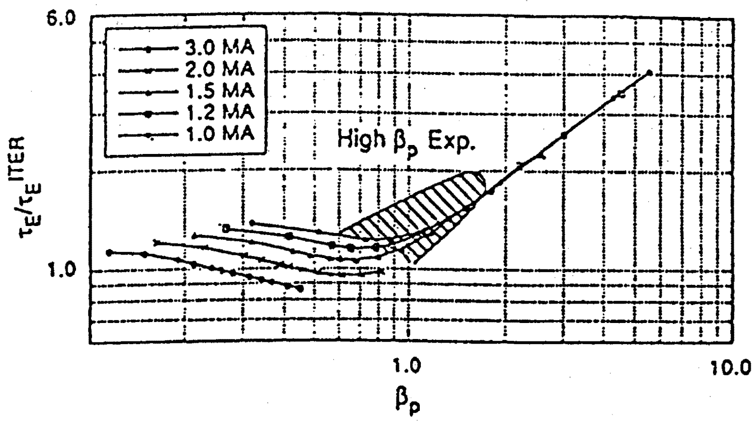


Fig. 5 Improvement factor of the energy confinement time $\tau_E/\tau_E^{ITER}$, is shown as a function of $\beta_p$ for various current and heating power (cited from Ref. [34] ).

of $\langle\sigma v\rangle$ is written as $\langle\sigma v\rangle_0\, g(T)$. The dimensionless function $g(T)$ is normalized to unity at the temperature $T=T_*$, where $T_*$is defined by $dg/dT_*=2.5g/T_*$ (typically $T_*\sim$(6-10)keV). Substituting Eq. (2.24) and $\langle\sigma v\rangle$ into Eq. (2.1), and setting $Q_{br}=0$, the energy balance equation is rewritten as

$$\frac{\partial}{\partial t}\frac{3}{2}n_eT=\frac{E_\alpha\langle\sigma v\rangle_0}{4}n_e^2g(T)-\frac{3n_eT^{2.5}}{2f_\tau^{2.5}LI_p^2(1+\beta_p^4)^{0.5}}. \tag{2.25}$$

The steady state solution is given by

$$I_p^2\left(1+\zeta\frac{T^4}{I_p^8}\right)^{0.5}=C_fT^{2.5}g(T)^{-1}, \tag{2.26}$$

where $\zeta$ and $C_f$ coefficients which depend on the density and size of the system, $\zeta=(8\pi^2a^2n_e/\mu_0)^4$ and $C_f=6/f_\tau^{2.5}n_eLE_\alpha\langle\sigma v\rangle_0$, respectively. In the limit of $\zeta=0$, relation (2.24) reduces the relation with L-mode confinement.

Figure 6 illustrates the phase diagram of the steady state solution in the plane of the plasma current $I_p$ and temperature $\langle T_D\rangle$(the volume averged deuteron temperature, i. e., $\langle T_D\rangle=T$ in this case) (cited from [35]). The density and other parameters are assumed to be constant. The dashed dotted line corresponds to the case of L-mode ($\zeta\sim0$, or $\beta_p\langle\langle 1$). The solid line is the case of finite $\zeta$ value. In this case, new branches (III and IV) appear in the lower current region besides the usual branches ( I and II). A solution of the approximate form $\sqrt{\zeta}\,T^2I_p$ holds in the low current limit. This solution gives the low temperature branch and the high temperature branch for a fixed plasma current, as is shown by the solid line in Fig. 6 (branches III and IV). The upper temperature branches (II and IV) represent the solution of the stable (and high fusion output) ignition states. The lower temperature branches ( I and III) show the

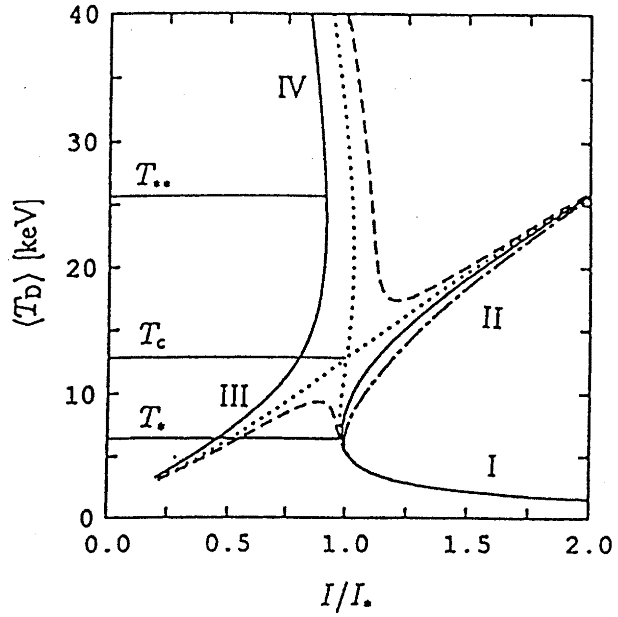


Fig. 6 Phase diagram in an ignited plasma. The stationary solution (solid line) is compared to that of an L-mode plasma (dashed dotted line). In addition to the usual branches I and II, new branches (III and IV) appear. When the finite $\beta_p$ improvement becomes strong, the branches merge (dotted lines), i.e., the stable branches II and IV become continuous (dashed lines), and the unstable branches I and III become continuous (cited from Ref. [35] ).

unstable (and low fusion output) ignition solutions.

When confinement enhancement by a bootstrap current is effective (i. e., $\xi$ is finite), branches I and II shift to the lower current side compared with the L-mode. In addition to this shift, the stable branches II and IV. and the unstable branches I and III become continuous (dashed lines). The two branches merge at the $T=T_*$. As mentioned above, merging of the L-mode branches with the high $\beta_p$-mode branches has a strong dependence upon the density. Taking the effect of the He-ash into account, we will descuss about this in Sec. III.

## II-4. The operational window for the self-ignited plasma

Considering the performance of the ITER-like plasma on the basis of the present data, it has been found the difficulty to achieve the high $Q$ value in L-mode plasma, where the $Q$ value is defined as the ratio of the released fusion energy to the input energy to plasma. Therefore improvement of $\tau_E$ is required.

Various improved confinement mode, such as H-mode, have been achieved in tokamaks. Accordingly, the plasma parameters are expected to be improved comparing with those in L-mode. In the burning plasma, however, it is not sufficient that only $\tau_E$ becomes longer. The plasma must be sustained steady, controllable by pumping sufficiently, and the wall must be endurable the heat flow from the burning region. To obtain the desirable performance, at least the above conditions should be satisfied.

On the basis of consistency-analysis, the operational window for the steady burning plasma which satisfies the following empirical constraints were evaluated at the stage of 1989 [36].

(1) The $\beta$ limit

$$\beta < \beta_c(\%) = G\frac{I_p}{aB_t}, \text{ with } G=2.7$$

where $\beta$ is defined by $\beta = 4\mu_0 n_e T/B_t^2$.

(2) The $q$ limit (which may lead to the current disruption)

$$q_{95} \geq 3.$$

(3) The density limit (which may lead to the density disruption)

$$\bar{n} < \bar{n}_c = 0.4\frac{I_p}{a^2}(0.1P_{in})^{\delta}, \text{with } \delta=0.25.$$

(4) The current drive-efficiency

$$I_p < \frac{C_I T}{n_e R}P_{in}, \text{ with } C_I = 0.026.$$

(5) The condition for the low temperature divertor

$$T_{div}\ eV = \frac{2.5\sqrt{P_{in}}}{n_e^2 \chi_{95} aR}, \text{ for } T_{div} < 10\text{eV},$$

where $\chi_{95}$ is plasma elongation.

(6) The condition for the He-ash pumping (a result for preliminary analysis)

$$\frac{n_e V}{\tau_p} > 10^4 S_\alpha,$$

where $V$ is the plasma volume, $\tau_p$ is the particle confinement time, $S_\alpha$ is $\alpha$-particle production rate.

(7) The energy confinement time is considered.
The power law scaling is given by

$$\tau^P{}_E = 0.103 M^{0.5} \chi_{95}^{0.25} I_p^{0.85} \bar{n}^{0.1} B_t^{0.3} a^{0.8} R^{0.5} P_{in}^{-0.5}.$$

(8) Extended JT-60 scaling law is used for the particle confinement time (which corresponds to $\tau_{\alpha 1}$ is Sec. II-2.),

$$\tau_p = 0.05\bar{n}^{-1}(B_t/4.5)^{\sigma}\ aP_{in}^{-0.5}, \text{ with } \sigma \sim 1.5.$$

Figure 7 shows the operational window on the $P_{in}$-$\bar{n}$ plane with power law scaling of energy confinement time $\tau_E$ for $I_p = 20$ MA (cited from [36]). Each of

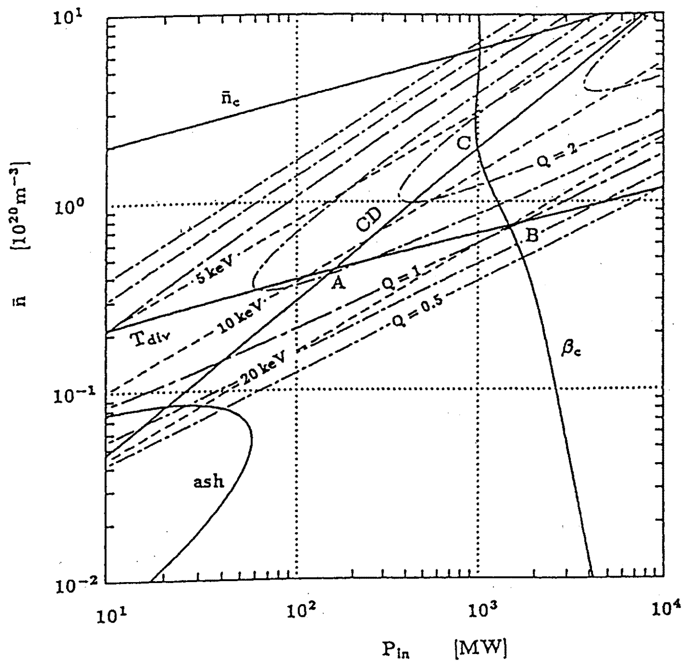


Fig. 7 The operational window in the $P_{in}-\bar{n}$ plane ($P_{in}$: input power, $\bar{n}$: line averaged density) with Power law of energy confinement time $\tau_E$ for $I_p$=20 MA Each of solid lines present the steady state conditions (1)~(6), dashed lines present the isothermal lines, dashed dotted lines present the iso-$Q$ lines (cited from Ref. [36] ).

solid lines presents the steady state condition (1)~(6), dashed line presents the isothermal line, dashed dotted line presents the iso-$Q$ line. In the case with $I_p$ =20 MA, the triangular region ABC in the range of 160 MW $< P_{in} <$ 1.5 GW, and $0.44\times10^{20}m^{-3} < \bar{n} < 1.9\times10^{20}m^{-3}$ is the steady state operational window. The operational point (A) for the minimum $P_{in}$ is determined by the condition of current drive (4) and the condition of low temperature divertor (5), i. e., $P_{in}$=160 MW, and $\bar{n}=0.44\times10^{20}m^{-3}$. In this operational point (A), parameters are given by $T$=11 keV, $\tau_E$=1.04 s, and $Q$=1.5. The required heating power $P_{in}$ to attain the maximum $Q$ value, which is limited by the $\beta$ limit (1), the current drive condition (4) is to be very large value : 1 GW. The condition for the ash-pumping given by (6) is satisfied easily.

## III. The effect of He-ash-poisoning on the L, high $\beta_p$-mode confinement

### III-1. Basic Equations and assumptions

In order to examine the ignition conditions of burning plasmas, we consider the deuterium (D) and tritium (T) mixture plasma where the $\alpha$-particles (He) exist as the product of fusion reactions. Their densities are denoted by $n_j$ (j= D, T, He, e). We consider the case where $n_D=n_T$ and $n_i=n_D+n_T$. The volume averaged temperature $T$ is assumed to be the same value among all species, for simplicity. It is assumed that $\alpha$ particles are fully thermalized without escaping from the plasma.

The energy balace equation and the particle balance equation are solved, based on the point model. In the energy balance equation, we specify the confinement mode by introducing the theoretically modeled scaling law of the energy confinement time $\tau_E$ [34].

From the condition of charge neutrality, the densities satisfy the following relations,

$$f_i=\frac{n_i}{n_e}=\frac{n_D+n_T}{n_e}=1-2f_{He}, \tag{3.1}$$

$$f_{tot}=\frac{1}{n_e}(n_e+n_i+n_{He})=2-f_{He}, \tag{3.2}$$

where $f_{He}$ indicates the ratio of helium density to electron density, $f_i$ is the ratio of ion density to electron density, and $f_{tot}$ is normalized to the electron density. In the ignition state, we consider the power balance equation where the power input from $\alpha$ particles (with $E_\alpha=3.52$ MA), the heat transport losses and the volume radiation losses are balanced as

$$\frac{\partial}{\partial t}\frac{3}{2}n_e f_{tot}T=\frac{1}{4}n_e^2 f_i^2 E_\alpha\langle\sigma v\rangle-\frac{3}{2\tau_E}n_e f_{tot}T-R_{rad}n_e^2, \tag{3.3}$$

where $\langle\sigma v\rangle$ indicates D-T reaction rate [37]. As for $\tau_E$, we employ Eq. (2.24) with the numerical constant $f_\tau^{2.5}L=2.4$.

It is assumed that the radiation loss is dominated by the bremsstrahlung. All the Gaunt factors are set to be unity, since they are insensitive for the variation of $T$ and are order unity. For the radiation loss rate $R_{rad}$, we use the expression

$$R_{rad}=f_i R_{b,1}(T)+f_{He}R_{b,2}(T) \qquad [keV\cdot m^3/s], \tag{3.4}$$

where $R_{b,1}(T)=3.34\times10^{-21}T^{1/2}$, and $R_{b,2}(T)=13.4\times10^{-21}T^{1/2}$.
The particle balance of He-ash is given by

$$\frac{\partial}{\partial t}n_e f_{He}=\frac{1}{4}n_e^2 f_i^2\langle\sigma v\rangle-\frac{1}{\tau_\alpha^*}n_e f_{He}, \tag{3.5}$$

where $\tau_\alpha^*$ is the global particle confinement time for He-ash [7]. Introducing the ratio of $\tau_E$ and $\tau_\alpha^*$, i. e., $\rho\equiv\tau_\alpha^*/\tau_E$, we shall examine the steady state condition of ignited plasma.

Substituting the scaling law of Eq. (2.24) into the energy balance Eq. (3.3), and setting $\partial/\partial t=0$, we obtain:

$$\hat{I}_p^4\left(1+\zeta\frac{\hat{T}^4}{\hat{I}_p^8}\right)=\left\{\frac{T^{2.5}\frac{3}{2}f_{tot}}{f_\tau^{2.5}L_{ne}I_p^{2*}\frac{1}{4}f_i^2E_\alpha\langle\sigma v\rangle-R_{rad}}\right\}^2, \tag{3.6.1}$$

with

$$\zeta=(8\pi^2a^2n_eT^*/\mu_0I_p^{2*})^4. \tag{3.6.2}$$

where $\hat{T}$ is normalized temperature using $T^*$ which satisfies the condition $d\langle\sigma v\rangle/dT=2.5\langle\sigma v\rangle/T$, (typically $T^*\approx10$ keV depending on the profile), and $\hat{I}_p$ is normalized current using $I_p^*(\equiv\sqrt{12T^{*2.5}/f_\tau^{2.5}n_eLE_\alpha\langle\sigma v\rangle_{T=T*},})$ which is determined from Eq. (3.6.1) with $\zeta=0$ and $\rho=0$. It should be noted that the definition of $\zeta$ is different from that in Sec. II by the factor $(T_*/I_{p*}^2)^4$. The value of $\zeta$ has the strong $n_e$ dependence as seen from Eq. (3.6.2).

Combining Eqs. (3.3) and (3.5) with $\partial/\partial t=0$, and using the relations (3.1) and (3.2), we obtain a following cubic equation for the helium concentration ratio $f_{He}$ [7],

$$a_0+a_1f_{He}+a_2f_{He}^2+a_3f_{He}^3=0, \tag{3.7}$$

where

$$a_0=-3T,\ a_1=\frac{27}{2}T+\frac{E_\alpha}{\rho}-\frac{4}{\langle\sigma v\rangle\rho}R_{b,1}(T),$$

$$a_2=-18T-\frac{4E_\alpha}{\rho}+\frac{4}{\langle\sigma v\rangle\rho}[2R_{b,1}(T)-R_{b,2}(T)],\ a_3=6T+\frac{4E_\alpha}{\rho}.$$

The solutions which satisfy the condition $0\leq f_{He}<0.5$ have physical meanings.

### III-2. Numerical results for burning performance

Solving Eq. (3.6.1) together with Eq. (3.7), we examine the predicted burning performances of the high $\beta_p$-mode as well as these of the L-mode. For given values of $E_\alpha$ and $\rho$, the fraction $f_{He}$ is determined through Eq. (3.7) as a function of the temperature.

Figure 8 shows the temperature dependence of $f_{He}$ for various values of $\rho$. For the fixed value of $T$, there are two solutions for $f_{He}$. For example, for the case with $T=30$ keV and $\rho=3$, $f_{He}=0.08$ and 0.37 are obtained. The line of $\rho=0$ an unrealistic boundary and the lines with $\rho\geq1$ have physical meaning. As $\rho$ increases, the working range of temperature becomes narrower. In the case with $\rho>15$, an operational window for the steady state condition vanishes, as was reported in Ref. [7].

Regarding the ignition condition, we obtain the relation $T=T(\hat{I}_p)$ for the steady solutions from Eq. (3.6.1), where we fix the value of $\zeta$ (or the averaged density $n_e$). The corresponding value of $f_i$ is obtained from Eq. (3.7). The effects of fuel dilution and radiation loss are taken into account in the steady states of the L-mode and the high $\beta_p$ mode confinements. If the relations $R_{b,1}(T)=R_{b,2}(T)=0$ and $f_{He}=0$ are assumed in Eq. (3.6.1), we recover the previous results

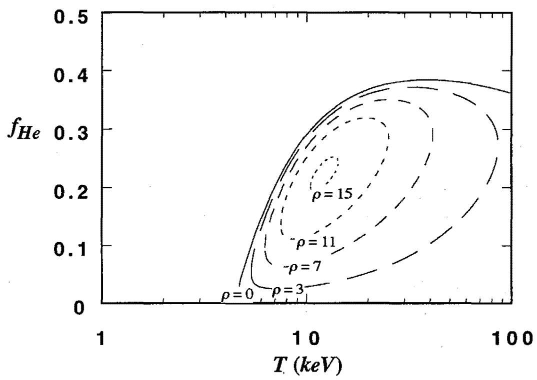


Fig. 8 The self-ignition conditions in the $T-f_{He}$ plane for $\rho$=0, 3, 7, 11, and 15. All the Gaunt factors are set to be unity. As the value of $\rho$ increases, the range of the allowed temperature and accessible ignition parameters are reduced.

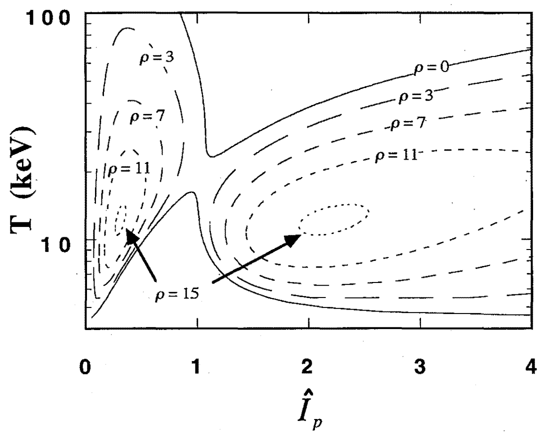


Fig. 9 The self-ignition conditions in the $\hat{I}_p-T$ plane for $\rho$=0, 3, 7, 11, and 15. The density parameter $\zeta$ is fixed to be 0.1. The higher current branches correspond to the L-mode, and the lower current branches correspond to the high $\beta_p$-mode. The divergence of the density does not occur for the case with finite $\rho$ value.

in Ref. [35]. The case with $\zeta=0.1$ is shown in Fig. 9. The contours drawn in the high current region ($\hat{I}_p>1$) correspond to the L-mode branches, and the contours in the low current region ($\hat{I}_p>1$) correspond to the high $\beta_p$ mode branches. As $\rho$ increases, the encircled region becomes narrower, and it will totally disappear when $\rho>\rho_{crit}\approx 15$. It is found that there is no divergence of the temperature for the high $\beta_p$-mode branch if the effects of fuel dilution and the radiation loss are simultaneously taken into account. On the other hand, without these effects, the divergence of the temperature occurs for the high $\beta_p$ mode branch [35]. This corresponds to the case with $\rho=0$ in Fig. 9.

The upper bound of $T$ decreases and the lower one increases as $\rho$ increases. The phase diagram of ignition contours shown in Fig. 9 is very sensitive to the change of the plasma density. If we increase the value of $\zeta$, i.e., accordingly $n_e$, we find that the merging starts between the L-mode and the high $\beta_p$-mode branches. The branches with low $\rho$ values are tend to be merged easily for the given density. In the high density region, the clear discrimination between the L-mode and the high $\beta_p$-mode disappears.

The core performance is evaluated by the associated helium contamination ratio $f_{He}$. In Fig. 10 we show the bird's-eye view of the performance among the contaminatio $f_{He}$, the temperature $T$ and the current $\hat{I}_p$ for $\zeta=0.1$. It is found that there are at most four solutions for $\hat{I}_p$ at fixed $T$, and the lowest cuttent solution and the highest current solution correspond to the upper bound of $f_{He}$.

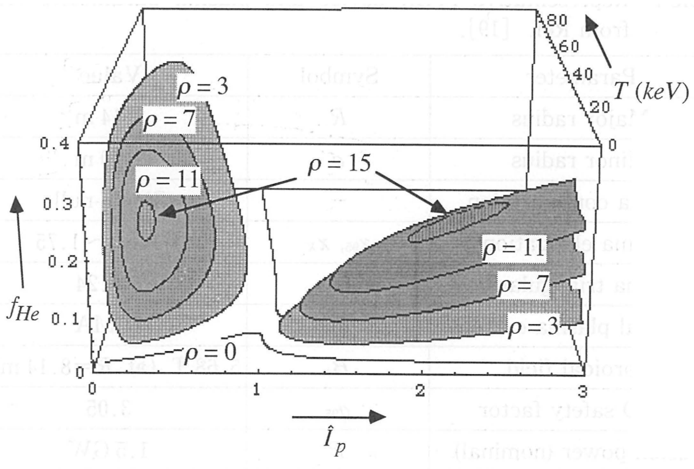


Fig. 10 The bird's-eye view of the self-ignition conditions among the Hecontamination $f_{He}$, the temperature $T$, and the current $\hat{I}_p$ for $\zeta=0.1$. There are four solutions for the current at a fixed plasma temperature.

### III-3. The burning performance of ITER-like plasmas

In Sec. II-4 the constraints originated from MHD instabilities on the steady state operation are discussed. In this section, three of them; the $\beta$ limit, the $q$ limit, and the density limit are examined as operational constraints. It is necessary for the steady state operation of the burning plasma to avoid the density disruption. The density limit is evaluated based on the empirical model such as Greenwald limit [45] or Borrass limit [46]. The former is given by $n_e < n_{ec} = I_p/\pi a^2$, which is somewhat different from the formula (3) discussed in II-4. The latter is derived on the basis of an energy balance at the plasma edge and is given by $n_e < n_e^{Borrass} = (1.4 \sim 2.4) \times 10^{20} m^{-3}$ for ITER parameters. We use these models for the evaluation of the density limit. We assume that the plasma has ITER-class parameters. The present status and expected performance of the ITER design has been reported (see Table 1) [19].

The high $\beta_p$ limit restricts the operation window for the high $\beta_p$-mode with high temperature, and/or with high density (or with low current). In the case of $\beta_p > R/a$, the plasma could be subject to the MHD instability [47] ; the case with $\beta_p < 2.9$ is believed to be stable for ITER parameters. Noting these operational limits, we examine the burning performance in the ITER-like plasma.

Figure 11 shows the ignition contour map in $I_p - T$ plane. For ITER-like parameters we calculate the ignition conditions from Eqs. (3.6.1) and (3.7) for various value of $\rho$. In Fig. 11 we plot the contours of the steady state solutions for different values of the density ; (11(a) ($n_e = 4.01 \times 10^{19} m^{-3}$), 11(b) ($n_e = 7.12 \times$

Table 1 Representative ITER device and plasma parameters cited from Ref. [19].

| Parameter | Symbol | Value |
|---|---|---|
| Major radius | $R$ | 8.14 m |
| Minor radius | $a$ | 2.80 m |
| Plasma configuration | — | Single-null |
| Plasma elongation | $\varkappa_{95}$, $\varkappa_X$ | ~1.6, ~1.75 |
| Plasma triangularity | $\delta_{95}$ | ~0.24 |
| Nominal plasma current | $I_p$ | 21 MA |
| Toroidal field | $B_t$ | 5.68 T (at $R$=8.14 m) |
| MHD safety factor | $q_{95}$ | 3.05 |
| Fusion power (nominal) | $P$ | 1.5 GW |
| Average wall loading | $\Gamma_n$ | ~1 MW/m |
| PF flux swing | $\Delta\phi_{PF}$ | 530 Wb |
| Flux swing for burn | $\Delta\phi_{burn}$ | 84 Wb |

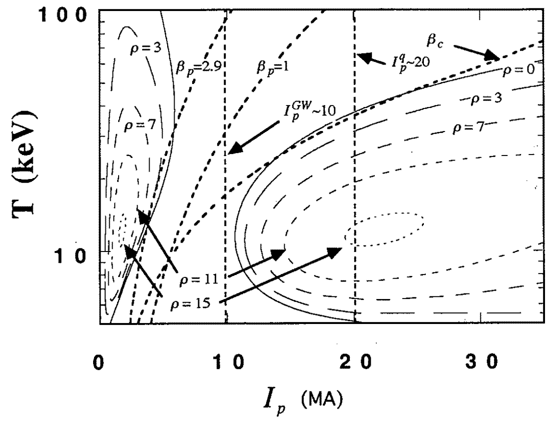


Fig. 11(a) The ignition contour of the ITER-like tokamak in the $I_p - T$ plane for $\rho=0$, 3, 7, 11, and 15. Parameters are $R=8.14$ m, $a=2.80$ m, $B=5.68$ T and $n_e=4.01\times10^{19}\ m^{-3}$. The lines for $I_p^{GW}\sim10.0$ MA $I_p^q\sim20$ MA, the $\beta$ limit $\beta_p=1.0$, and 2.9 are also shown. Most of the high $\beta_p$-mode branches are located above the high $\beta_p$ limit ($\beta_p=2.9$), and all the solutions for the high $\beta_p$-mode are unstable for the Greenwald limit.

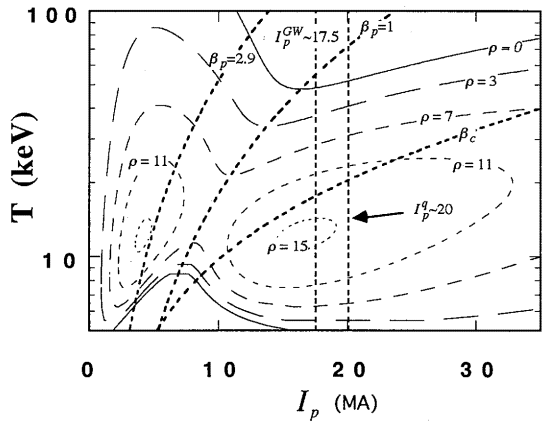


Fig. 11(b) The ignition contour of the ITER-like tokamak in the $I_p - T$ plane for $\rho=0$, 3, 7, 11, and 15. The density is fixed as $n_e=7.12\times10^{19}\ m^{-3}$, and other parameters are the same as those for Fig. 11(a). The lines for $I_p^{GW}\sim17.5$ MA, $I_p^q\sim20$ MA, the $\beta$ limit $\beta_p=1.0$, and 2.9 are also shown. The high $\beta_p$-mode branches are unstable for the Greenwald limit.

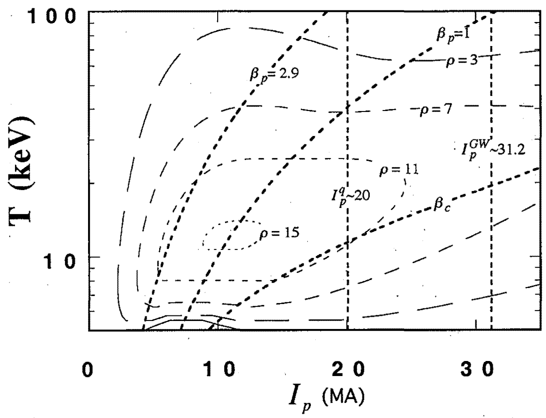


Fig. 11(c) The ignition contour of the ITER-like tokamak in the $I_p-T$ plane for $\rho$=0, 3, 7, 11, and 15. The density is fixed as $n_e$=1.27 $\times10^{20}\,m^{-3}$, and other parameters are the same as those for Fig. 11(a). The branches of $\rho$=15 merge. The lines for $I_p^{GW}\sim$31.2 MA, $I_p^q\sim$20 MA, the $\beta$ limit $\beta_p$=1.0, and 2.9 are also shown.

$10^{19}m^{-3}$) and 11(c) ($n_e=1.27\times10^{20}m^{-3}$)). Using the relation $\beta_p^4\equiv\zeta\hat{T}^4/\hat{I}_p^2$, or $\hat{T}\beta_p\hat{I}_p^2/\zeta^{1/4}$, lines of $\beta_p$=2.9 and $\beta_p$=1.0 are drawn for the given value of $n_e$. In the low density case : $n_e=4.01\times10^{19}m^{-3}$, the high $\beta_p$-mode braches for the finite value of $\rho$ are located above the high $\beta_p$ limit. In this density range, the high $\beta_p$ -mode branch and the L-mode branch are well separated as seen from Fig. 11(a). The separation becomes clearer for the larger value of $\rho$. The Greenwald density limit $n_e\langle n_{ec}=I_p/\pi a^2$ is reinterpreted as the lower bound of the current (i. e., the plasma is stable if $I_p\rangle I_p^{GW}$) and is shown is Fig. 11. The $\beta$ limit and the $q$ limit ($q_{95}\geq3$, i. e., the plasma is stable in)$I_p\rangle I_p^q\sim$20 MA for ITER-like plasma [19]) are also plotted. The current is constrained by the Greenwald limit and the $q$ limit such that $I_p^{GW}\langle I_p\langle I_p^q$, where $I_p^{GW}\equiv\pi a^2n_e\sim$10 MA and $I_p^q\sim$20MA. We find that the branch of the high $\beta_p$-mode, which corresponds to the region sandwiched between $\beta_p$=2.9 and $\beta_p$=1.0 does not lie in the region $I_p^{GW}\langle I_p\langle I_p^q$. The branch of L-mode corresponds to the right hand side region of $\beta_p$=1 line, lies in this region.

As the averaged density increases, the high $\beta_p$ and L-mode branches start to merge and finally they become the same branch. These are seen in Fig. 11(b) and Fig. 11(c). In the case with $n_e=7.12\times10^{19}m^{-3}$ (Fig. 11(b)), the high $\beta_p$-mode branches with $\rho\leq7$ merge with those of the L-mode. In this case, the lower bound of the current is $I_p^{GW}\sim$17.5 MA and the upper bound of the current is $I_p^q$ $\sim$20 MA. The condition $I_p^{GW}\langle I_p\langle I_p^q$ restricts only to the L-mode operation. In the case with $n_e = 1.27 \times 10^{20} m^{-3}$ (Fig. 11(c)), all branches of the L-mode and the high $\beta_p$-mode merge into closed lines. We do not see the clear discrimination between the L-mode and the high $\beta_p$-mode. The region $I_p^{GW} < I_p < I_p^g$ does not exist, however the operational window can be found, if we employ the Borrass model. At present, there is no dependable scaling law for the density limit, the decisive conclusion can not be drawn.

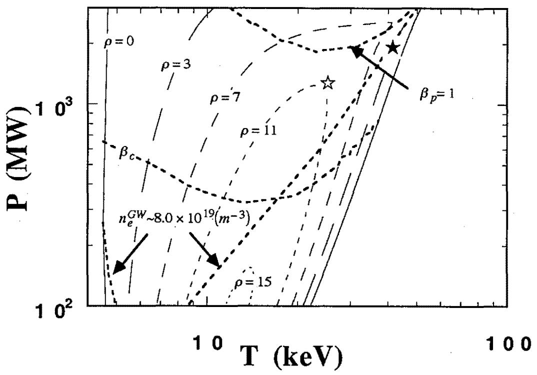


Fig. 12(a) The ignition contour of the ITER-like tokamak in the $T-P$ plane for $\rho=0$, 3, 7, 11, and 15. The plasma current is fixed as $I_p=20$ MA (the L-mode operation). The lines for $n_e^{GW} \sim 8.0 \times 10^{19} m^{-3}$, the $\beta$ limit, and $\beta_p=1.0$ are also shown.

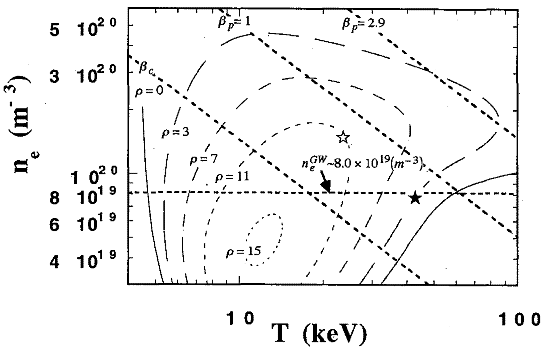


Fig. 12(b) The ignition contour of the ITER-like tokamak in the $T-n_e$ plane for $\rho=0$, 3, 7, 11, and 15. The plasma current is fixed as $I_p=20$ MA (the L-mode operation). The lines for the Greenwald limit; $n_e^{GW} \sim 8.0 \times 10^{19} m^{-3}$, the $\beta$ limit, $\beta_p=1.0$, and 2.9 are also shown.

Next, we examine the temperature dependence of the fusion power for both the L-mode and the high $\beta_p$-mode.

The nominal plasma current for ITER is reported to be 21MA. We choose the parameters to distinguish the confinement mode as $I_p$=20MA for the L-mode and $I_p$=10MA for the high $\beta_p$-mode, respectively. The fusion power $P$ is calculated according to the following formula as

$$P=\frac{1}{4}n_e^2(1-2f_{He})^2\langle\sigma v\rangle E_n V, \tag{3.9}$$

where $E_n$ is the energy of neutron (14.1MeV).

Figure 12 shows the ignition contours, on $P$(MW)$-T$(KeV) plane. The case with $I_p$=20MA for various values of $\rho$ is shown (Fig. 12(a)). The corresonding density is calculated from Eq. (3.6.1) as a function of $T$, $I_p$ and $\rho$. The line of $\beta_p=1$ is also plotted. In the case with $I_p$=20MA, the Greenwald limit is $n_e^{GW}=8.0\times10^{19}m^{-3}$, which is indicated by the dotted line. The ignition contours on $n_e-T$ plane for $I_p$=20MA are shown in Fig. 12(b). Let us show the examples of the burning performances of the points marked by ☆ and ★ in Fig. 12(a) and (b). The point marked by ☆ corresponds to a high $\rho$ value operation ($\rho$=11) and has the performance $P\sim$1.3 GW, $n_e\sim1.6\times10^{20}m^{-3}$, $T\sim$23 keV, $f_{He}\sim$31 %, $\beta_p\sim$0.7, $\beta_p\sim$4.5 %, and $\tau_E\sim$8.7s, for a high current operation (L-mode operation), The point marked by ★ corresponds to a typical low $\rho$ value operation ($\rho$=3). The performance is that $P\sim$2.0GW, $n_e\sim8.0\times10^{19}m^{-3}$, $T\sim$42keV, $f_{He}\sim$10 %, $\beta_p\sim$0.6 %, $\beta\sim$4.2 % and $\tau_E\sim$3.5s, for this operation. The $\beta$ limit is 3.39 % in these cases. Although the value of $\beta$ exceeds the $\beta$ limit for these parameters, the operations in the second stability regime could be possible therefore we leave the argument on the $\beta$ limit undone.

Figure 13(a) shows the ignition contours of the solutions on $P$(MW)$-T$(keV) plane for the case with $I_p$=10MA for various values of $\rho$. The contours on $n_e-T$ plane are shown in Fig. 13(b). In the case with $I_p$=10MA, the Greenwald limit is nearly equal to $n_e^{GW}=4.0\times10^{19}m^{-3}$ as is shown in Fig. 13(b) by the dotted line. The burning performance at the operational point marked by ☆ and ★ in Fig. 13(a) and 13(b) are explicitly shown. The high $\rho$ value operation ($\rho$=11) marked by ☆ gives $P\sim$0.86GW, $n_e\sim1.14\times10^{20}m^{-3}$, $T\sim$25keV, $f_{He}\sim$28 %, $\beta_p\sim$2.3, $\beta\sim$3.6 % and $\tau_E\sim$12s, for $I_p$=10MA. The operational point is located above the critical density $n_e^{GW}$, but is below $n_e^{Borrass}$ Presently the fusion power for ITER is anticipated to be $P\sim$1.5GW [1]. It is found to be difficult for high $\beta_p$-mode operation with high $\rho$ value. The point marked by ★($\rho$=3) has the performance, for this operation $P\sim$1.6GW, $n_e\sim7.0\times10^{19}m^{-3}$, $T\sim$53keV, $f_{He}\sim$13 %, $\beta_p\sim$2.9, $\beta\sim$4.6 % and $\tau_E\sim$5.3s. The $\beta$ limit is 1.69 % in these cases.

## Ⅳ. Summary and Discussion

We surveyed the previous analyses of the thermal instability. Based on a point model, we discussed the thermal stability. We briefly discussed about the

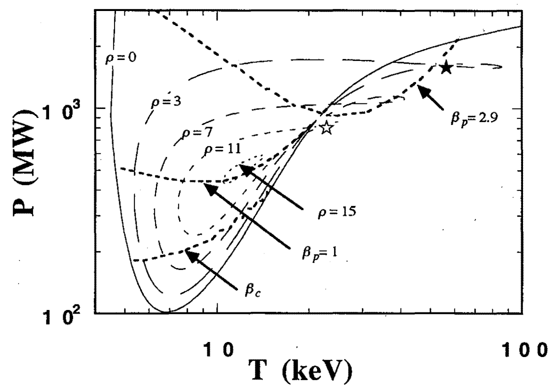


Fig. 13(a) The ignition contour of the ITER-like tokamak in the $T-P$ plane for $\rho=0$, 3, 7, 11, and 15. The plasma current is fixed as $I_p=10$ MA (the high $\beta_p$-mode operation). The lines for the $\beta$ limit, $\beta_p=1.0$, and 2.9 are also shown.

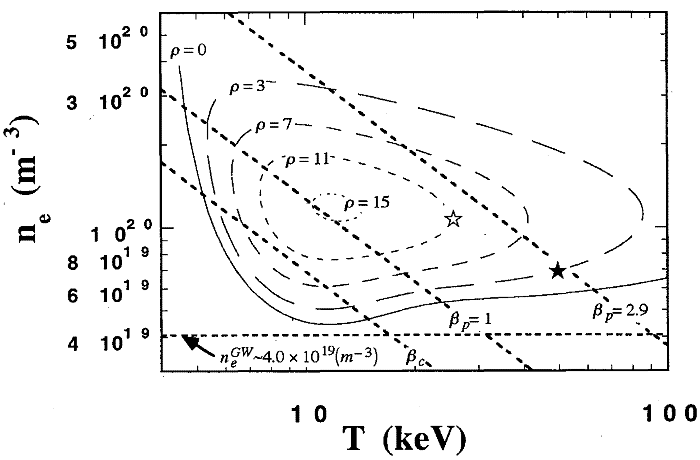


Fig. 13(b) The ignition contour of the ITER-like tokamak in the $T-n_e$ plane for $\rho=0$, 3, 7, 11, and 15. The plasma current is fixed as $I_p=10$ MA (the high $\beta_p$-mode operation). The lines for the $\beta$ limit, $\beta_p=1.0$, and 2.9 are also shown. All ignition contours are above the Greenwald limit; $n_e^{GW}\sim4.03\times 10^{19}\ m^{-3}$.

confinement problem of fast $\alpha$-particle and He-ash, and reviewed previous analysis in which He-ash contamination is introduced consistently. Characteristic energy confinement time for the L-mode and the high $\beta_p$-mode were introduced. And some constraints to burning operation are shown.

The effect of He-ash-poisoning which includes both the effects of fuel dilution and radiation losses was analyzed in the steady states of the L-mode and the high $\beta_p$-mode confinements in Sec. III. Regarding the ignition condition, we obtained the $\hat{I}_p - T$ relation and found that as the value of $n_e$ increases, the high $\beta_p$-mode branches merge with the L-mode branches. The branches with low $\rho$ values merge at low density. As $\rho$ increases, the region, which has the consistent steady state solution, becomes narrower for all parameters, and it totally disappears for $\rho > \rho_{crit} \approx 15$ even for the high $\beta_p$-mode. The devergence of the temperature which has been predicted in the absence of ash-poisoning is not observed for the case of the reasonably finite $\rho$ value.

For ITER-like plasma we firstly investigated the operational window for the self-ignited plasma, considering the high $\beta_p$ limit, the $\beta$ limit, the $q$ limit, and the density limit. We showed the burning performance for three different cases of the density, plotting the ignition conditions for various values of $\rho$. We also compared the temperature dependence of the fusion power for both the L-mode and the high $\beta_p$-mode in ITER-like plasma, choosing the parameters to distinguish the mode as $I_p$=20MA for the L-mode and $I_p$=10MA for the high $\beta_p$-mode, respectively.

Another scenario for ITER is to operate at ELMy-H mode. We show the burning performance of the ELMy-H mode for the reference. The global scaling of energy confinement time for the ELMy-H mode is given as follows [48],

$$\tau_E^{ELMy} = 0.032 I_p^{0.63} B_t P_{in}^{-0.53} M^{0.33} R^{2.52} n_e^{0.26} \varepsilon^{0.33} \chi_{95}^{0.46}, \tag{3.10}$$

where $\varepsilon$ is the inverse plasma aspect ratio, and the empirical scaling of the threshold power for L-H transition [49] is given by

$$P_{H-threshold} \approx 0.3 \bar{n} B_t R^{2.5}. \tag{3.11}$$

Substituting Eq. (3.3), the igntion condition is obtained. In Fig. 14, the ignition contours for the ELMy-H mode on $P$(MW)$-T$(keV) plane is shown. The dashed lines are also shown which correspond to the power threshold of L-H transition [49], and the Greenwald limit ($\sim 8.0 \times 10^{19} m^{-3}$), and $\beta_p$=1 are also shown, respectively. The burning performance at the point marked by ★ is $P \sim$2.2GW, $n_e \sim 8.0 \times 10^{19} m^{-3}$, $T \sim$58keV, and $f_{He} \sim$15 %, $\beta_p \sim$0.9, $\beta \sim$5.7 % and $\tau_E \sim$5.4s for $\rho$=3, and the point marked by ☆ has the performance of $P \sim$2.2GW, $n_e \sim 2.2 \times 10^{20} m^{-3}$, $T \sim$24keV, and $f_{He} \sim$25 %, $\beta_p \sim$1.0, $\beta \sim$6.6 % and $\tau_E \sim$7.0s for $\rho$=11. The point marked by ☆ is above the Greenwald limit. Comparing these two cases, power output are nearly equal. If a higher density operation than the Geeenwald limit is possible, ELMy-H mode seems to be a candidate of operation mode.

We in this paper presented the ignition conditions where both effects of the

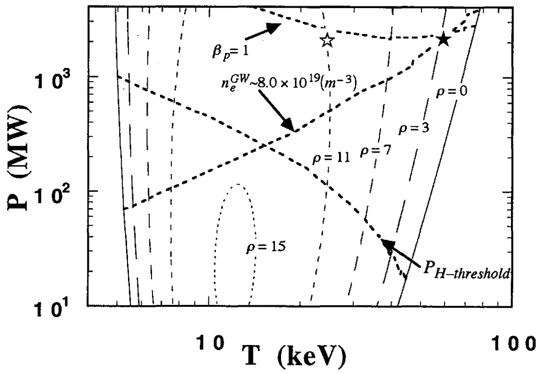


Fig. 14 The ignition contour of the ITER-like tokamak in the $T-P$ plane for $\rho=0$, 3, 7, 11, and 15. The plasma current is fixed as $I_p=20$ MA. The global scaling of energy confinement time for ELMy-H mode is used. The lines for $P_{H\text{-threshold}}$, and $\beta_p=1.0$ are also shown.

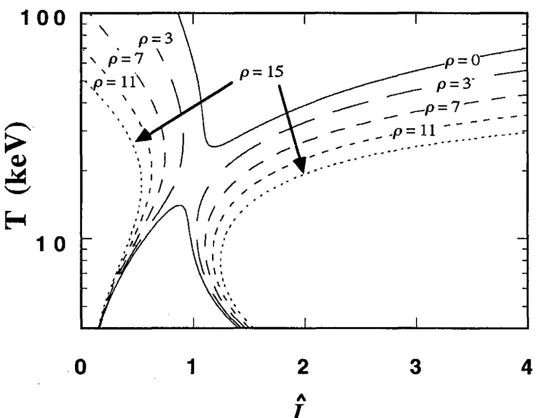


Fig. 15 The effect of fuel dilution (the radiation loss is excepted) on the self-ignition condition in $\hat{I}_p - T$ plane for $\rho=0$, 3, 7, 11, and 15. The density parameter $\zeta$ is fixed to be 0.1. The higher current branches correspond to the L-mode, and the lower current branches correspond to the high $\beta_p$-mode.

fuel dilution and the radiation energy loss are retained. For the reference, we here show the result where only the effect of fuel dilution is taken into account in the L-mode and the high $\beta_p$-mode operation. The case with $\zeta=0.1$ is plotted in Fig. 15. The curve $\rho=0$ reduces to the results of Ref. [35]. Comparing with the results in Fig. 9, we see that contours are not closed in the absence of the effect of radiation loss due to He-ash and fuel ions.

We assumed that the fast $\alpha$-particles can be confined perfectly and fully thermalized before they lose their energy. However if the D-T reaction occurs frequently and the interaction among fast $\alpha$-particles comes to nontrivial, the effective confinement of $\alpha$-particles can not be insured. This problem needs further analysis for the transport of plasma. This is left for our future work.

**Acknowledgments**

Authors heartily wish to thank Prof. K. Itoh for his guidance and stimulating discussions and Prof. A. Fukuyama for useful discussions.

**References**

[1] M. Ohta, H. Yamato, S. Mori, Plasma Physics and Controlled Nuclear Fusion Research (Proc. 4th Int. Conf. Madison, 1971). vol. 3, IAEA, Vienne 423 (1971)
[2] L. Bromberg, J. L. Fisher, D. R. Conn, Nucl. Fusion 20 (1980) 203.
[3] M. Okamoto, M. Ohnishi, J. Nuc. Sci. Tech. 20 (1983) 366.
[4] M. Ohnishi, A. Saiki, M. Okamoto, Nuclear Technology/Fusion 5 (1984) 326.
[5] K. Tani et al., Fusion Technology 18 (1990) 625.
[6] Y. Nakamura, H. Nishihara and M. Wakatani, Nucl. Fusion 26 (1986) 907.
[7] D. Reiter, G. H. Wolf, H. Kever, Nucl. Fusion 30 (1990) 2141.
[8] W. Bieger, K. H. Dippel, G. Fuchs, G. H. Wolf, in Plasma-Wall Interactions (Proc. Int. Symp. Julich, 1976), Pergamon Press, Oxford (1976) 609.
[9] M. Kaufmann, K. Lackner, J. Neuhauser, H. Vernickel, Nucl. Fusion 25 (1985) 89.
[10] O. Mitarai, A. Hirose, H. M. Skarsgard, Nucl. Fusion 28 (1988) 2141.
[11] N. A. Uckan, J. S. Tolliver, W. A. Houlber, S. E. Attenberger, Fusion Technol. 13 (1988) 411.
[12] R. J. Bickerton, Bull. Am. Phys. Soc. 349 (1989) 2145.
[13] A. D. Cheetham, A. Gondhalekar, J. C. M. De Haas, et al., in Plasma Physics and Controlled Nuclear Fusion Research 1988 (Proc. 12th Int. Conf. Nice, 1988), Vol. 1, IAEA, Vienna (1989) 483.
[14] INTOR GROUP, International Tokamak Reactor, Zero Phase (Rep. Int. Workshop Vienna, 1979), IAEA, Vienna (1995) 247.
[15] R. V. Budny, et al., Nucl. Fusion 35 (1995) 1497.
[16] M. P. Petrov, et al., Nucl. Fusion 35 (1995) 1437.
[17] S. J. Zweben, et al., Nucl. Fusion 35 (1995) 893.
[18] M. H. Redi, et al., Nucl. Fusion 35 (1995) 1509.
[19] ITER-JCT and Home Teams, Plasma Phys. Control. Fusion 37 (1995) 140.
[20] Ya. I. Kolesnichenko, Nucl. Fusion 20 (1980) 727.
[21] R. J. Goldston, Plasma Phys. Control. Fusion 26 (1984) 87.
[22] P. Yushmanov, T. Takizuka, K. S. Riedel, O. J. W. F. Kardaun, S. M. Kaye and

D. E. Post, Nucl. Fusion 30 (1990) 1999.
[23] M. Kikuchi et al., Fusion Eng. Design 16 (1991) 253.
[24] S. Ishida et al., in Plasma Physics and Controlled Nuclear Fusion Research 1992 (Proc. 14th Int. Conf. Wurzburg, 1992), Vol. 1, IAEA, Vienna 219 (1993).
[25] Y. Koide et al., Phys. Rev. Lett. 72 (1994) 3662 : Y. Koide et al., in Plasma Physics and Controlled Nuclear Fusion Research 1994 (Proc. 15th Int. Conf. Seville, 1994), paper IAEA-CN-60/A-2-I-3.
[26] C. D. Challis et al., Nucl. Fusion 33 (1993) 1097.
[27] M. Keilhacker and JET TEAM, in Plasma Physics and Controlled Nuclear Fusion Research, Vol. 1 15 (1992).
[28] M. C. Zarnstorff et al., in Plasma Physics and Controlled Nuclear Fusion Research, Vol. 1 (1992) 111.
[29] JT-60 TEAM et al., in Plasma Physics and Controlled Nuclear Fusion Research Vol. 1 (1992) 57.
[30] EQUIRE TORE SUPRA, in Plasma Physics and Controlled Nuclear Fusion
[31] K. Itoh, S-I. Itoh, and A. Fukuyama, Phys. Rev. Lett. 69 (1992) 1050.
[32] K. Itoh, S-I. Itoh, A. Fukuyama, M. Yagi and M. Azumi, Plasma Physics and Controlled Nuclear Fusion Research 1992 (Vienna : IAEA) Vol. 2 p381 ; 1993 Plasma Phys. Control. Fusion 35 543.
[33] A. Fukuyama, K. Itoh, S-I. Itoh, M. Yagi and M. Azumi, Plasma Phys. Control. Fusion 36 (1994) 1385.
[34] A. Fukuyama, K. Itoh, M. Yagi, M. Azumi, Plasma Phys. Control. Fusion 37 (1995) 611.
[35] A. Fukuyama, S.-I. Itoh, M. Yagi, K. Itoh, Nucl. Fusion 35 (1995) 1669.
[36] S.-I. Itoh, A. Fukuyama, T. Takizuka, K. Itoh, Fusion Technol. 16 (1989) 346.
[37] T. Takizuka and M. Yamagiwa, JAERI-M 87-066 (1987).
[38] M. Kikuchi, M. Azumi, S. Tsuji, K. Tani and H. Kubo, Nucl. Fusion 30 (1990) 343.
[39] J. G. Cordey and JET Team, Plasma Physics and Controlled Nuclear Fusion Research 1992 Vol. 2 (Vienna : IAEA) p161.
[40] A. Taroni, M. Erba, E. Springmann and F. Tiborn, 1993 Proc. 20th European Conf. on Controlled Fusion and Plasma Physics (Lisbon) Vol 17C, ptI, p72.
[41] M. Yagi, K. Itoh, S-I. Itoh, A. Fukuyama and M. Azumi, 1993 Phys. Fluids B5 3702 ; 1994 J. Phys. Soc. Japan 63 10
[42] B. Coppi, A. Frreira, J. W-K. Mark and J. J. Ramos, Plasma Phys. Control. Fusion 5 (1979) 1.
[43] T. Morishita, A. Fukuyama and Y. Furutani, J. Phys. Soc. Jpan 57 (1988) 1238.
[44] F. L. HInton and R. D. Hazeltine, Rev. Mod. Phys. 48 (1988) 239.
[45] M. Greenwald et al., Nucl. Fusion 28 (1988) 2199.
[46] K. Borrass et al., Nucl. Fusion 33 (1993) 63.
[47] S. Ishida et al., Phys. Rev. Lett. 68 (1992) 1531.
[48] F. Ryter, H mode database working group, Nucl. Fusion 36 (1996) 1217.
[49] H mode database working group, Nucl. Fusion 34 (1994) 131.

(Received May 8, 1997)